JOURNAL OF GUIDANCE, CONTROL, AND DYNAMICS
Vol. 18, No. 6, November–December 1995

Maximum-Payload Trajectories for a Laser-Propelled Launch Vehicle

W. Edward Humble* and Bion L. Pierson†
Iowa State University, Ames, Iowa 50011-3231

The feasible trajectories of a laser-propelled launch vehicle are restricted by the laser power available, the power lost to atmospheric absorption and beam spreading, and the thruster design. These constraints result in optimal trajectories that are significantly different from those for conventional launch vehicles. The problem formulation and constraints for a launch vehicle using a pulsed-laser thruster with two laser power transmission models are presented. A maximum payload problem for launch to various circular orbits is solved for both transmission models using sequential quadratic programming. An unusual backswing trajectory feature is obtained for most of the optimal trajectories presented. The optimal trajectories for various circular orbit altitudes are discussed, and the effects of altering the power transmission efficiency are shown.

I. Introduction

LASER-PROPELLED launch vehicles were first proposed in the early 1970s.[1] Advances in laser and optics technology since then have increased the feasibility of very high power, ground-based, laser launch systems.[2,3] Such systems offer the potential of thousands of launches to low Earth orbit (LEO) per year at greatly reduced costs over current launch vehicles.[4]

Kantrowitz[5] has proposed an extremely simple (and hence cheap) design for a laser-propelled launch vehicle. The vehicle is essentially a right circular cone of some solid propellant with a payload in the apex as shown in Fig. 1. The conical shape allows the vehicle to turn relative to the laser beam without exposing the payload to the laser. When struck by a double-pulsed laser beam, the entire base of the vehicle acts as a double-pulse planar thruster (DPPT) as described by Kare.[4] A low-power pulse evaporates a desired amount of propellant from the thruster surface to form a thin layer of gas. The gaseous propellant is then heated by a laser-supported detonation (LSD) wave initiated and sustained by a second, high-power laser pulse. The hot gas then expands one dimensionally producing thrust.

This thruster design has several important characteristics. The thrust is always perpendicular to the surface, independent of the angle of incidence of the laser. This allows the thrust vector to be aimed off the axis of the laser beam. In addition, the available thrust is dependent only on the amount of laser energy striking the vehicle and the thruster efficiency. Thus, the thruster can be throttled by adjusting the energy and duration of the laser pulse. However, the laser power striking the thruster must be enough to induce an LSD wave. If the power drops below 10^7 W/cm^2, no LSD wave is formed, and the thrust produced is negligible. Finally, such a vehicle could theoretically be controlled from the ground by altering the power distribution across the laser pulse. This would generate torques for controlling the attitude and therefore thrust direction of the vehicle. This greatly reduces the complexity of the launch vehicle.

Because of these unusual characteristics, it is expected that the optimal trajectories for such a launch vehicle would be significantly different from those for more conventional systems. Chern et al.[6] have studied optimal vertical ascent trajectories to geosynchronous Earth orbit (GEO), but they neglect laser power losses due to range and atmosphere. Kare[7] has developed a detailed laser propulsion model that includes atmospheric absorption losses, diffraction losses, and the geometry constraints placed on a double-pulse planar thruster. He has used computer simulation to study the performance of this type of laser-propelled launch vehicle using a simple, fixed guidance scheme, but no optimal trajectories were obtained.

In this paper, a similar laser launch system is modeled. Kare's[7] flat Earth geometry and constant drag coefficient are replaced with partially spherical Earth dynamics and analytical functions for aerodynamic lift and drag. Sequential quadratic programming (SQP)[8] is used to numerically solve a maximum payload-to-orbit optimal control problem (OCP). The two-dimensional maximum payload trajectories to various circular orbits are presented for two laser power transmission models, and the unique aspects of these trajectories are discussed.

II. Problem Formulation

The launch system model for this research is based on work done by Kare[7] at Lawrence Livermore National Laboratory. Propulsion

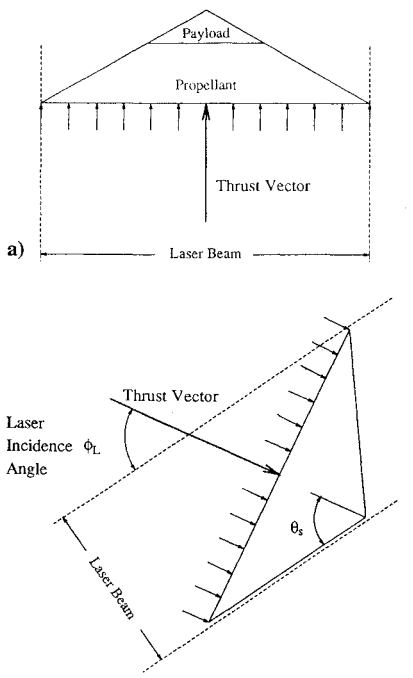

Fig. 1 Laser-propelled launch vehicle. Laser incidence angles up to the semivertex angle θ_s are allowed.

Received Oct. 14, 1993; revision received Feb. 1, 1995; accepted for publication March 18, 1995.

*Graduate Student, Department of Aerospace Engineering and Engineering Mechanics; currently Engineer, United Engineering Co., Imperial, MO 63052.

†Professor, Department of Aerospace Engineering and Engineering Mechanics. Associate Fellow AIAA.

Table 1 Vehicle characteristics and initial conditions

Average laser power P_{av}, W	300 (10^9)
Peak laser power P_{peak}, W	300 (10^{12})
Laser wavelength λ, μm	10.6
Mirror radius r_m, m	5
Laser site altitude h_L, m	3000
Minimum laser flux on thruster ϕ_{min}, W/m^2	10^{11}
Atmospheric absorption coefficient α, m^{-1}	1.25 (10^{-5})
Atmospheric scale height h_0, m	8000
Reference atmospheric density ρ_0, kg/m^3	1.225
Vehicle base radius r_{vhl}, m	0.75
Vehicle semivertex angle θ_s, deg	55
Thruster efficiency η_{thr}	0.40
Thruster exhaust velocity c, m/s	8000
Turnover time T_{to}	0.30
Initial altitude h_0, m	3050
Initial surface range x_0, m	0
Initial velocity V_0, m/s	10
Initial flight-path angle γ_0, deg	90
Initial mass m_0, kg	1900

is provided by a single ground-based laser with 300 MW average power P_{av} and a 10.6 μm wavelength λ. The laser emitter is assumed to be located on a 3000-m mountain peak to put it above the thickest part of Earth's atmosphere and thus increase the transmission efficiency. The system launches a DPPT-powered vehicle with an initial mass m_0 of 1900 kg and a semivertex angle θ_s of 55 deg. Some launcher mechanism is assumed to impart a small altitude and velocity to the vehicle before turning on the laser.

Since they are more interesting and harder to achieve, only launches to a circular orbit are presented. Both minimum time- and maximum payload-to-orbit optimal solutions have been obtained.[9] However, the optimal trajectories for both performance indices are nearly identical in most cases, due to the difficulty of achieving circular orbit. Thus, only the maximum payload-to-orbit solutions will be presented here.

Equations of Motion

The vehicle dynamics are the standard planar, point-mass equations of motion[10] over a nonrotating, flat Earth with inverse-square gravity field and a stationary, exponential atmosphere (see Fig. 2). The state variables are altitude h, surface range x, velocity V, flight-path angle γ, and vehicle mass m. The steering angle δ is a control variable. The dynamic equations are

$$\dot{h} = V\sin\gamma \tag{1}$$

$$\dot{x} = [R_e/(R_e + h)]V\cos\gamma \tag{2}$$

$$\dot{V} = [T(x,h)\cos\delta - D - W\sin\gamma](1/m) \tag{3}$$

$$\dot{\gamma} = [T(x,h)\sin\delta + L - W\cos\gamma](1/mV) \tag{4}$$

$$\dot{m} = -\frac{T(x,h)}{c} \tag{5}$$

The initial conditions and vehicle characteristics are summarized in Table 1.

Vehicle Aerodynamics

The equations for aerodynamic lift L and drag D are only a rough approximation based on Newtonian impact theory for hypersonic velocities.[11] This approximation yields an analytical aerodynamic model that depends explicitly on the semivertex angle θ_s and the angle of attack. However, since thrust is always perpendicular to the base of the cone, the angle of attack is always equal to δ (see Fig. 2). The expressions for lift and drag become

$$L = \frac{\rho(h)V^2A_{vhl}}{2}(C_{norm}\cos\delta - C_{axial}\sin\delta) \tag{6}$$

$$D = \frac{\rho(h)V^2A_{vhl}}{2}(C_{norm}\sin\delta + C_{axial}\cos\delta) \tag{7}$$

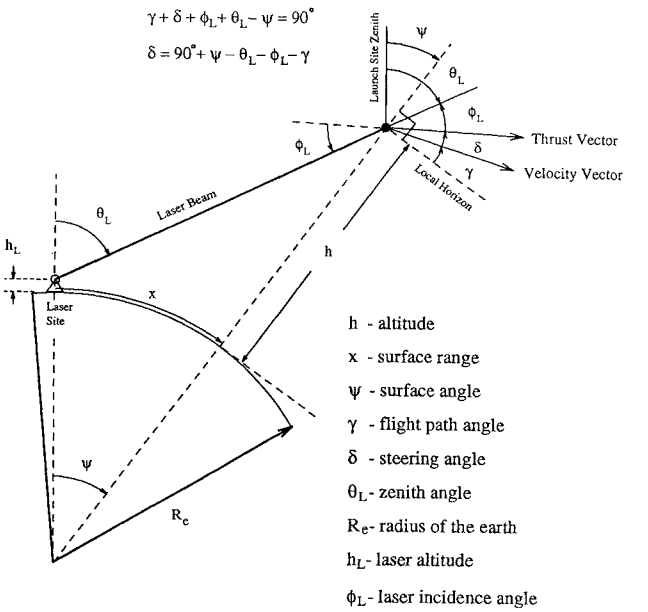

Fig. 2 Launch vehicle flight geometry.

where

$$C_{axial} = 2\sin^2\theta_s + \sin^2\delta\left(1 - 3\sin^2\theta_s\right)$$

$$C_{norm} = \sin 2\delta\cos^2\theta_s$$

$$A_{vhl} = \pi r_{vhl}^2$$

$$\rho(h) = \rho_0 e^{-h/h_0}$$

Thruster Model

The thruster is assumed to convert a percentage of the laser power striking the thruster P_{thr} into kinetic energy in the exhaust. Thus,

$$T(x,h) = \frac{2\eta_{thr}P_{thr}(x,h)}{c} \tag{8}$$

where

$$\eta_{thr} = 0.40$$

Thruster efficiency η_{thr} and exhaust velocity c are assumed to be constants for the entire trajectory. Although small-scale tests have only resulted in efficiencies of 10%,[4,12] it is expected that much higher efficiencies are practical for larger lasers and longer pulses. The 40% thruster efficiency is a nominal value set by the Strategic Defense Initiative Organization (SDIO) Laser Propulsion Program[13] based on theoretical models and experimental results.

Transmission Models

The laser power P_{thr} is determined by the losses in the laser beam as it travels to the vehicle. Thus,

$$P_{thr} = \eta_{trans}P_{av} \tag{9}$$

where the total transmission efficiency η_{trans} of the laser beam is a function of vehicle position. Two transmission models are used in this research.

Model 1

Model 1 is a simple model developed as a first step for this research. It uses an arbitrary expression for power transmission efficiency based on observation of the diffraction term presented in Kare's simulation results.[7] The power transmission efficiency η_{trans} is scaled to yield 70% transmission at some scaling range R_p:

$$\eta_{trans}(R) = 1 - 0.30\frac{R(x,h)^2}{R_p^2} \tag{10}$$

The effects of varying R_p from 650 to 1000 km have been investigated, and a nominal value of $R_p = 800$ km has been chosen. This model provides excessively high transmission efficiencies for very large zenith angles. This fault is partially addressed by adding a zenith angle constraint to the problem formulation.

Model 2

Model 2 uses the more realistic equations for the power transmission efficiencies derived by Kare.[7] The total power loss is divided into two parts: energy lost to atmospheric absorption and energy lost to beam spreading, or diffraction losses. The net transmission efficiency is $\eta_{\text{trans}} = \eta_{\text{atm}}\eta_{\text{diff}}$.

The atmospheric absorption coefficient η_{atm} has the form[7]

$$\eta_{\text{atm}} = e^{-\alpha \ell} \tag{11}$$

where α is the atmospheric absorption coefficient and ℓ is the effective path length through the atmosphere. An expression for ℓ is derived by integrating the unit atmospheric density along the laser beam's path. For a geometrically flat Earth[7]

$$\ell = \int_{h_L}^{h} \frac{e^{-(h/h_0)}}{\cos\theta_L}\,dh = \frac{h_0}{\cos\theta_L}\left[e^{(-h_L/h_0)} - e^{(-h/h_0)}\right] \tag{12}$$

where h_0 is the atmospheric scale height and h_L is the altitude of the laser site. It can be shown that the flat Earth result is a conservative approximation of the actual spherical Earth η_{atm}.[9] Because of the difficulty of calculating the actual spherical Earth η_{atm}, Eq. (12) is used for model 2.

The diffraction efficiency η_{diff} is due to the laser beam spreading as it travels to the vehicle and is approximated using[7]

$$\eta_{\text{diff}}(R) = 1 - 4\left[\frac{R(x,h)}{R_0}\right]^2 \tag{13}$$

where R_0 is a characteristic range given by $R_0 = 2\pi r_m r_0/\lambda$, r_m is the size of the main mirror, λ is the laser wavelength, and r_0 is the characteristic thruster radius based on the peak power available and the minimum flux $\phi_{\min}$ required to sustain an LSD wave: $r_0 = [P_{\text{peak}}/(\pi\phi_{\min})]^{1/2}$.

Laser Power Constraint

Since an LSD wave is required to generate significant thrust, P_{thr} must never fall below the level needed to initiate one. Based on the initial vehicle base area A_{vhl}, the minimum value is $P_{\text{thr}} = A_{vhl}\,10^{11}$ W/m^2. Comparing this with P_{av}, the necessary inequality constraint can be written

$$P_{\text{thr}}(x,h) - 0.589P_{\text{av}} \geq 0 \tag{14}$$

Figure 3 shows the area within which this constraint is satisfied for each model.

Zenith Angle θ_L Constraint for Model 1

As mentioned earlier, model 1 uses a simplified power transmission model that ignores the effects of atmospheric absorption on the laser beam. This results in very high transmission efficiencies for very large zenith angles that must be limited by applying a zenith angle constraint. Thus, for model 1 only, the inequality constraint

$$65 \text{ deg} - |\theta_L(t)| \geq 0 \tag{15}$$

where the maximum θ_L of ± 65 deg is chosen based on Kare's simulations.[7]

Laser Incidence Angle Constraint

For the DPPT to function, the laser must strike the thruster surface. In addition, the payload must be shielded from the laser beam to prevent damage. The conical shape of the vehicle allows this as long as the laser incidence angle ϕ_L never exceeds θ_s (see Fig. 1). Thus, the inequality constraint

$$\theta_s - |\phi_L(t)| \geq 0 \tag{16}$$

must be included in the problem formulation.

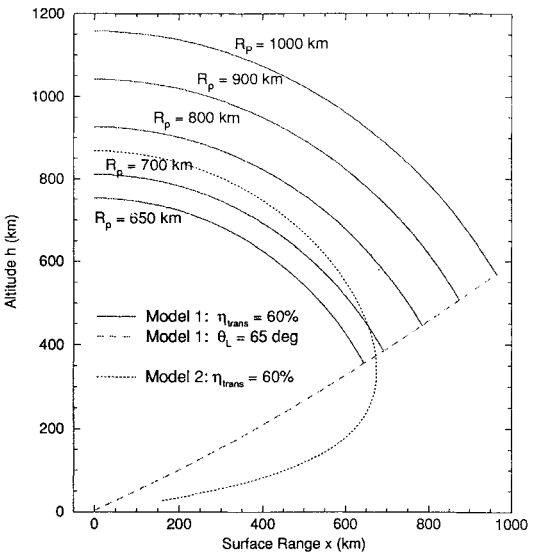

Fig. 3 Comparison of model 1 (R_p = 800 km) and model 2 flight envelopes.

Circular Orbit Constraints

The desired circular orbit is completely defined by its orbital altitude h_f. This allows meaningful conclusions to be drawn about the laser-propelled launch vehicle's performance as vehicle characteristics such as vertex angle or initial mass are changed. Three terminal equality state constraints specify a given circular orbit:

$$h(t_f) = h_f \tag{17}$$

$$\gamma(t_f) = 0 \text{ deg} \tag{18}$$

$$V(t_f) = \sqrt{\frac{\mu}{R_e + h_f}}, \qquad \mu = 398601.2 \text{ km}^3/\text{s}^2 \tag{19}$$

Laser Incidence Angle as the Control

Physically, the vehicle would be controlled from the ground by changing the steering angle δ. However, $\delta(t)$ is bounded by the laser incidence angle constraint, which is a function of the steering angle and position [see Fig. 2 and Eq. (20)]. Thus, the upper and lower bounds on the steering angle are time-varying functions that are dependent on $\delta(t)$ and the position of the vehicle:

$$\delta = 90 \text{ deg} + \psi(x) - \theta_L(x,h) - \phi_L - \gamma \tag{20}$$

where

$$\psi(x) = \frac{x}{R_e}$$

$$\theta_L(x,h) = \sin^{-1}\left[\frac{(R_e + h)\sin\psi(x)}{R(x,h)}\right] \tag{21}$$

$$R(x,h) = \sqrt{(R_e + h)^2 + (R_e + h_L)^2 - 2(R_e + h)(R_e + h_L)\cos\psi(x)}$$

On the other hand, the laser incidence angle ϕ_L is bounded by the constant θ_s of the conical vehicle. Since the steering angle can be easily calculated from a given ϕ_L and the state variables, the optimal control problem can be simplified by replacing δ in the equations of motion with ϕ_L as the bounded control variable. This incorporates Eq. (16) into the OCP as a simple control inequality constraint instead of a more difficult to implement state-variable inequality constraint.

Turnover Time

While the launch vehicle model was being validated, it was discovered that the vehicle is extremely sensitive to perturbations in ϕ_L (and thus in δ) during the first 2 min of flight. The velocity during

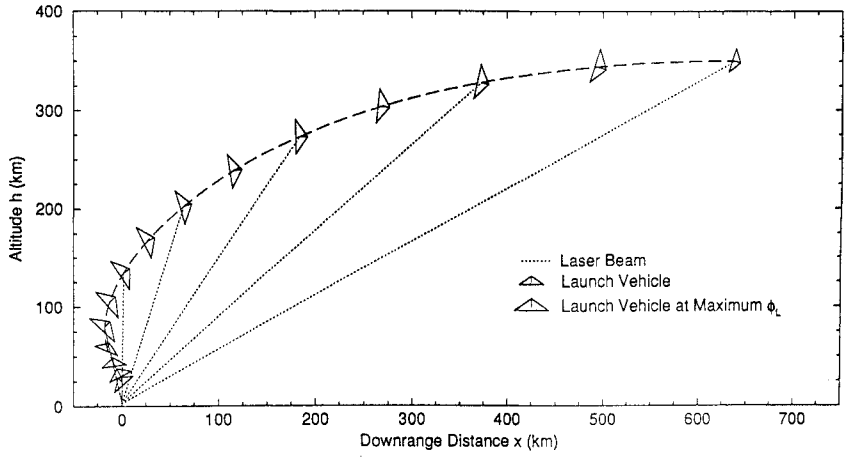

Fig. 4 Model 1: typical backswing trajectory, h_f = 350 km and R_p = 700 km.

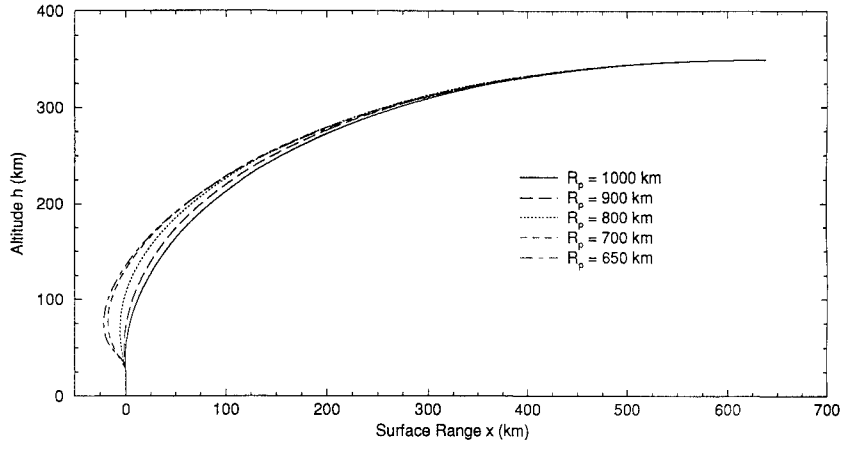

Fig. 5 Model 1: optimal trajectories to a 350-km circular orbit for various R_p.

this period is relatively low due to high atmospheric drag and a low initial thrust-to-weight ratio. Control perturbations tend to cause the vehicle to tip over and crash into the ground, thus causing problems for the SQP software. To eliminate this problem, a nondimensional turnover time T_{to} was added to the problem formulation. The control ϕ_L is set to zero for all times less than T_{to}. This constrains the initial part of the trajectory to a vertical climb, giving the vehicle more altitude and velocity before ϕ_L is allowed to vary. After studying the effects of turnover time on the performance index for model 1, we chose a nominal, nondimensional value of $T_{to} = 0.30$ to be used for all of the solutions presented here.

Optimal Control Problem Statement

The optimal control problem for a maximum payload-to-orbit launch can now be stated as follows: Find the bounded control $\phi_L(t)$, $0 \leq t \leq t_f$, that minimizes the performance index

$$J = -m(t_f)$$

subject to the control constraints

$$-\theta_s \leq \phi_L(t) \leq +\theta_s$$

the equations of motion (1–5) with the initial conditions given in Table 1, the inequality constraints (14) and (15) (this is only a constraint for model 1), and the terminal equality constraints (17–19).

Problem Solution Method

To solve this optimal control problem, the continuously time-varying control $\phi_L(t)$ is replaced with a vector of discrete control points and a linear interpolation process. To allow the time of flight t_f to vary, a linear time transformation $t = \alpha_t \tau$ is used to convert the free end-time optimal control problem into a fixed end-time problem by adding the time parameter α_t to the vector of design variables. The transformed differential equations can now be integrated over the fixed τ interval [0, 1]. The results presented here are for 22 design variables: 13 control points placed every 0.025 nondimensional time units starting from $\tau = T_{to} = 0.30$, followed by 8 control points placed every 0.05 time units, plus the parameter α_t.

The parameterized optimal control problem is now solved using an SQP routine.[14] Implementation of this algorithm requires a numerical integration method, in this case a fourth-order, fixed-step, Runge–Kutta method using 1000 steps. The performance index and constraints are evaluated after the integration process.

The constraint (14) on laser power reaching the thruster must be enforced over the entire trajectory. However, in practice the laser energy reaching the vehicle is monotonically decreasing, so the power constraint (14) is treated as a terminal state constraint. The ϕ_L constraint (16) is applied along the entire flight path by placing upper and lower bounds on each ϕ_L control point. With linear interpolation between the control points, $\phi_L(t)$ will never exceed its limits.

III. Model 1 Results—Backswing

Model 1 was initially used to determine the effect of turnover time T_{to} on the optimal trajectories. As expected, the payload-to-orbit increases with decreasing T_{to}. However, although $T_{to} = 0$ should give the maximum payload-to-orbit, the additional mass saved becomes negligible for $T_{to} \leq 0.30$. When $T_{to} \approx \leq 0.20$, the optimal trajectories do not show any significant differences.[9] Based on this work, a nominal T_{to} of 0.30 has been chosen and is used for all the results presented here.

The final position and velocity vectors of the launch vehicle are completely specified by the circular orbit and zenith angle

constraints. Since the vehicle turning rate is restricted by the ϕ_L constraint, the feasible trajectories are limited. To arrive at the desired location with the desired velocity, the vehicle makes use of a unique feature called a backswing as shown in Fig. 4. At turnover, ϕ_L jumps to a negative value, briefly tilting the vehicle uprange. It then increases until $\phi_L = \theta_s$. This curving flight path keeps the vehicle closer to the laser, thus increasing the available thrust and allowing the zenith angle constraint to be satisfied.

The laser transmission efficiency is the driving factor behind the backswing. As R_p is reduced, the available thrust at a given range from the laser decreases as well. To maintain sufficient thrust to satisfy the circular orbit constraints, the vehicle must stay closer to the laser to receive the same amount of laser energy. This leads to an increase in the magnitude of the backswing as shown in Figs. 5 and 6. Note from Fig. 6 that for the largest values of R_p the backswing is virtually nonexistent. The very high η_{trans} gives the vehicle enough thrust to easily satisfy the constraints. However, as R_p decreases, the magnitude of the backswing increases. This keeps the vehicle closer to the laser to maintain the needed thrust level.

Figure 7 shows that the negative ϕ_L at turnover increases with the increasing backswing. At the same time, the rate at which ϕ_L goes to the upper bound increases. This occurs because the vehicle must turn more sharply to fly through the backswing and accelerate to orbit.

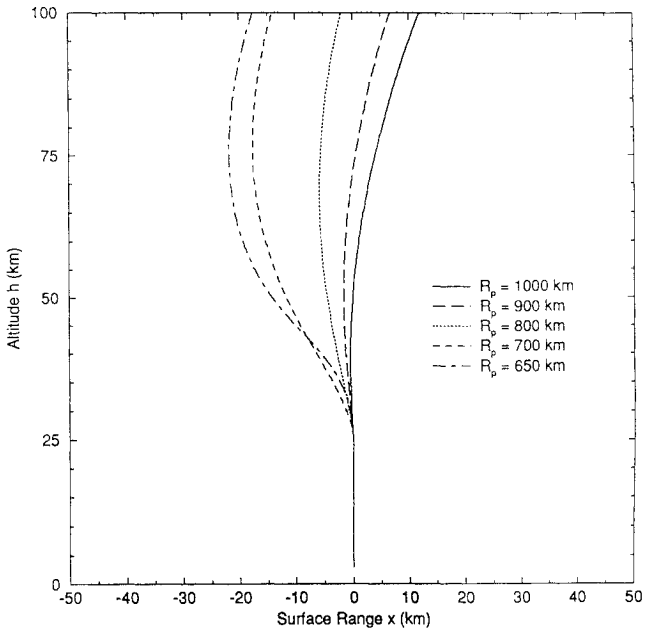

Fig. 6 Model 1: close-up of optimal trajectories to a 350-km circular orbit for various R_p.

This is expected since the lower scaling ranges force the vehicle to achieve orbit before it is carried beyond the zenith angle constraint, and this requires that the vehicle begin the downrange acceleration as soon as possible.

IV. Model 2 Results

The combined effects of the atmospheric and diffraction loss terms as the vehicle position changes can be seen in Fig. 3. Directly above the laser site, η_{trans} behaves like model 1 losses and falls off slowly. This is a result of the laser passing through only a small amount of the atmosphere. However, the atmospheric losses grow rapidly as zenith angle increases, and the laser power constraint curve sweeps sharply back toward the launch site, giving the vehicle an elliptical area in which it must achieve circular orbital conditions.

The inclusion of atmospheric losses significantly decreases the overall transmission efficiency of the problem and increases the difficulty of reaching orbital conditions. With the reduced laser power reaching the thruster, maintaining the power necessary to produce an LSD wave becomes much more difficult, and the inequality constraint on P_{thr}, Eq. (14), becomes active. This eliminates the need for the zenith angle constraint, which is now removed. Figure 3 shows the relative size and shape of the flight envelope for both models. Although the zenith angle constraint for model 1 restricts the vehicle's final position more than the model 2 envelope, the power delivered to the vehicle falls off more rapidly for combined atmospheric and diffraction losses, making model 2 more restrictive.

The maximum payload-to-orbit for these trajectories (see Fig. 8) behaves as would normally be expected; it decreases with increasing h_f, due to the extra fuel expended to lift the vehicle to the desired final altitude. However, at very low final orbit altitudes, the payload-to-orbit again decreases. The maximum final mass occurs when $h_f = 325$ km. Figure 3 shows that below this altitude the curve of minimum η_{trans} sweeps back toward the launch site, decreasing the maximum allowable surface range. With less room to reach circular orbit conditions, it is not surprising that the maximum payload-to-orbit decreases, since the vehicle must turn more sharply to make it to orbit and expends extra fuel. At this point, the final mass begins to decrease, giving this power-loss model and vehicle configuration an optimal circular orbit altitude for maximizing the payload-to-orbit.

The time-to-orbit (see Fig. 8) for these maximum payload trajectories shows a minimum time-to-orbit for $h_f = 310$ km. Below this altitude the trajectory must turn so sharply that the extra thrust gained no longer offsets the time required to fly through the backswing. It is important to note, however, that from $h_f = 330$ km down to the minimum altitude the time-to-orbit varies by less than a quarter-second. This points up the relative unimportance of the time-to-orbit, especially compared with the maximum payload-to-orbit problem.

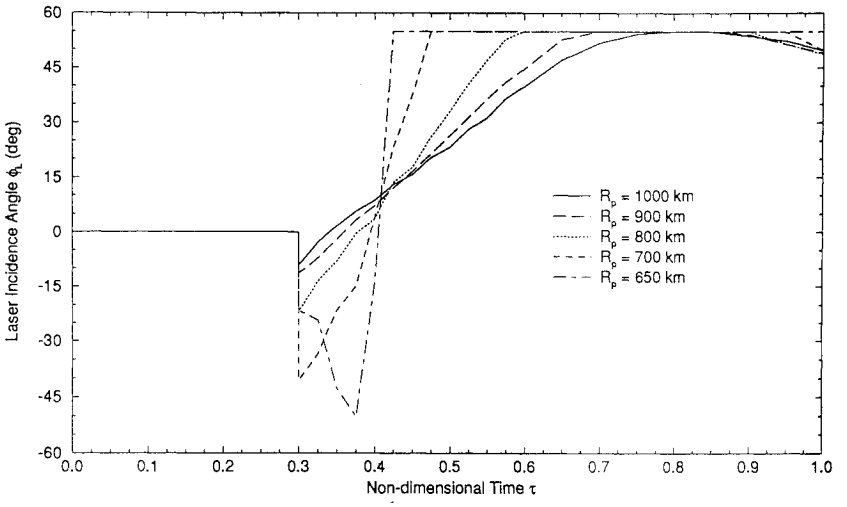

Fig. 7 Model 1: optimal ϕ_L histories for various R_p.

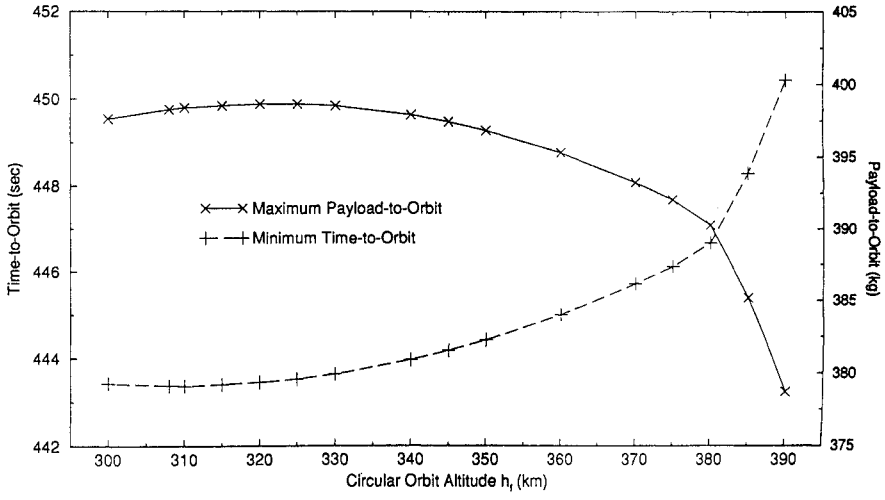

Fig. 8 Model 2: maximum payload-to-orbit and corresponding time-to-orbit for various h_f.

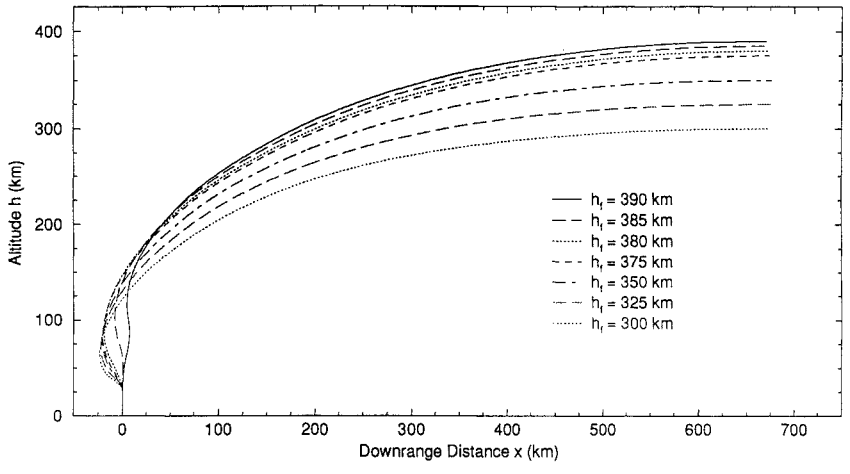

Fig. 9 Model 2: optimal trajectories for various h_f.

For circular orbit altitudes below 375 km, the trajectories are good examples of the typical backswing as shown in Figs. 9 and 10. As h_f decreases, the magnitude of the backswing slowly increases. The larger backswing reduces the vertical velocity of the vehicle so that it rises exactly to the desired final altitude, while keeping the vehicle as close to the laser as possible for the horizontal acceleration. The increasing payload-to-orbit for decreasing h_f observed in Fig. 8 is a result of the backswing that allows the vehicle to reach orbit more quickly and the decreasing final altitude that requires less fuel for the vehicle to achieve.

The optimal laser incidence histories (see Fig. 11) are similar to those previously observed for a backswing trajectory. The optimal ϕ_L spikes to a large negative value, followed by a rapid increase to the upper limit of +55 deg. As the circular orbit altitude decreases and the backswings become larger in magnitude, both the magnitude of the negative spike at turnover and the rate at which ϕ_L goes to the upper limit increase. The vehicle turns more and more sharply as h_f decreases, until for the lowest circular orbit possible ϕ_L goes to the lower limit (−55 deg) at turnover, holds there for a short time, then jumps almost directly to the upper limit, and holds there for most of the rest of the trajectory. Near the end of each of these optimal trajectories, the ϕ_L decreases from the upper limit. This change in ϕ_L guides the vehicle to the desired circular orbit by slowing the rotation rate of the velocity vector so that it exactly reaches zero just as the vehicle reaches the end of the flight. If ϕ_L instead remained on the upper bound until the end of the trajectory, γ would be negative. Only when the vehicle is at the upper limits of its performance ($h_f \geq 380$ km) does the optimal ϕ_L remain on the upper bound until the final time.

Figure 9 also shows the optimal trajectories that result for various final circular orbit altitudes greater than 375 km. These trajectories are at the upper limit of h_f for this vehicle configuration and show some unusual characteristics. When $h_f = 390$ and 385 km, the trajectories weave back and forth as they climb before turning downrange for the acceleration to orbital velocity. For $h_f = 380$ km the flight path looks more like the typical backswing trajectory seen previously, but Fig. 10 shows that it too has slight weaving visible right after turnover. As the final orbital altitude decreases to 375 km, the weaving disappears into the familiar pure backswing trajectory. This transition is due to the severe restrictions on the vehicle's final location, altitude, velocity, and flight-path angle.

As the desired orbital altitude increases, the maximum downrange distance decreases due to the constraint on η_{trans} (see Fig. 3). The vehicle must still meet the criteria for circular orbit, but it has less room to do so. Therefore a larger backswing is needed to keep the vehicle closer to the laser during the downrange acceleration, but a smaller backswing is needed to give the vehicle enough vertical velocity to rise to the desired altitude. Thus, a different type of trajectory is required to reach orbital conditions.

Figure 12 shows the vertical velocity component vs the vehicle's altitude. Except for differences caused by the different final altitudes, the velocity profiles are similar for each h_f, despite the very different flight paths the vehicle actually follows. Each trajectory gives the vehicle a vertical velocity just sufficient to lift it to the specified orbit. The two weaving trajectories are controlling their vertical velocity component by rotating the velocity vector. This is the only way the velocity can be controlled since there is no throttling on the laser power. Thus, when the vehicle finally turns downrange for the acceleration to orbital velocity, it has both the required vertical velocity profile to exactly lift it to the desired h_f, and it is also close enough to the laser site to receive the necessary laser power to accelerate to the required circular orbital velocity. This makeshift

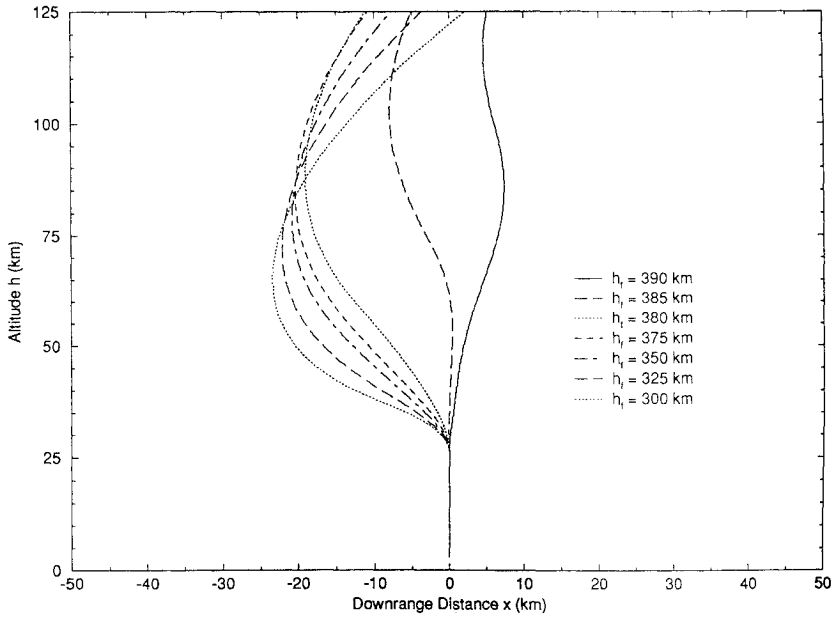

Fig. 10 Model 2: close-up of optimal trajectories for various h_f.

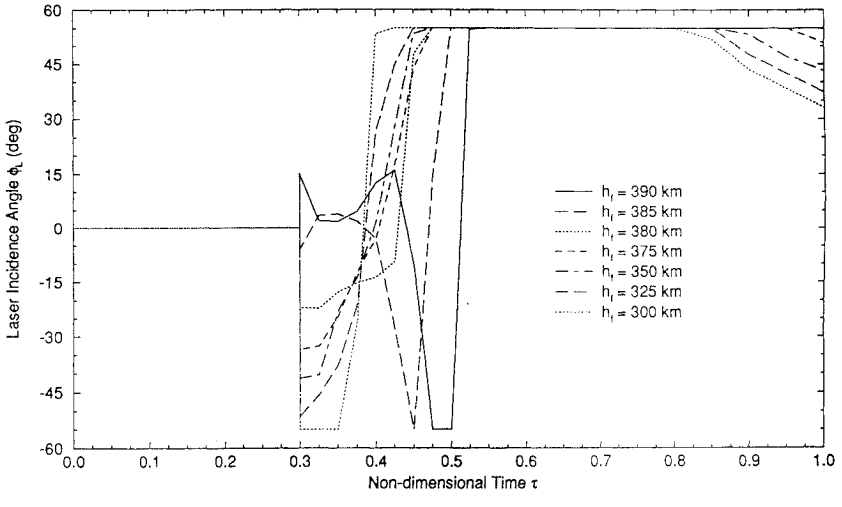

Fig. 11 Model 2: optimal ϕ_L histories for various h_f.

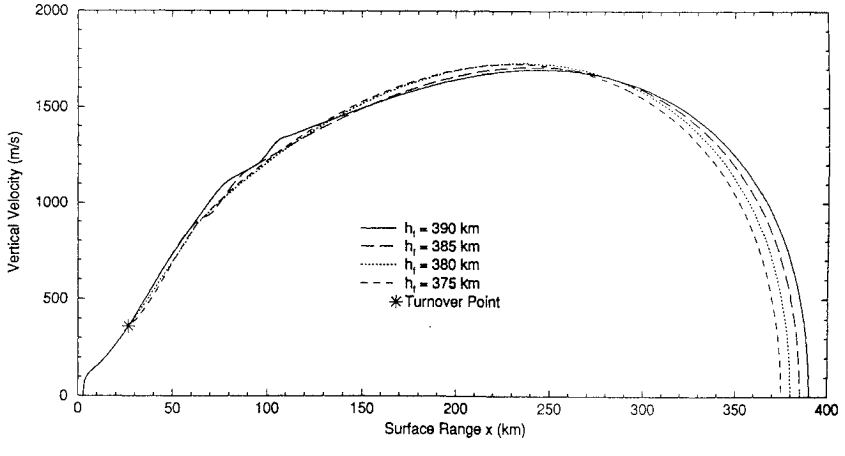

Fig. 12 Model 2: vertical velocity vs altitude for large (≥375 km) h_f.

throttling is expensive in terms of fuel but expands the range of circular orbits the vehicle can achieve.

The optimal ϕ_L history (see Fig. 11) reflects the rapidly changing trajectory types. For $h_f = 390$ km, ϕ_L oscillates between +15 deg and near 0 deg, drops to the negative limit, and then rises again to the positive limit where it stays for the rest of the trajectory. At $h_f = 385$ km ϕ_L oscillates only once before decreasing to $-\theta_s$ and then rising to $+\theta_s$ for the rest of the trajectory. The transition to a typical backswing trajectory (like that for $h_f = 375$ km) occurs when $h_f = 380$ km. This trajectory has a slightly atypical ϕ_L history where the rapid increase to the positive ϕ_L limit is delayed. This increases the height of the backswing, allowing the vehicle to reach the desired altitude. For $h_f \leq 375$ km, the ϕ_L histories are those of typical backswing trajectories with increasing backswing magnitudes.

V. Conclusions

For the first time, optimal launch-to-orbit trajectories have been obtained for a laser propulsion system. The two key features of the laser-propelled launch vehicle are the dependence of thrust on vehicle location and the constraint on vehicle attitude, and therefore thrust direction, relative to the laser. These factors severely limit the feasible launch trajectories and lead to an unusual backswing in most of the optimal trajectories. This feature is unique to laser propulsion and demonstrates the driving importance of the laser power losses on the optimal trajectory.

Furthermore, there is an optimum circular target orbit altitude for a given vehicle/laser configuration. This is a result of the extremely high turn rate the vehicle must use to successfully reach orbit. The tight turns burn extra fuel and require more velocity to be gained during the horizontal acceleration. This leads to a decrease in payload and an increase in time of flight for the lowest feasible circular orbits.

In future studies, we hope to determine the effects of changing the cone angle of the vehicle and varying the laser power during the launch. The weaving trajectories obtained for higher circular orbit altitudes indicate that the addition of throttle control to the problem could further expand the feasible circular orbit range. Improved aerodynamic models and the use of multiple laser sites should also be explored.

Acknowledgment

This research was presented as Paper AAS-95-117 at the 5th Annual AAS/AIAA Space Flight Mechanics Conference, Albuquerque, NM, Feb. 13–16, 1995.

References

[1]Kantrowitz, A. R., "Propulsion to Orbit by Ground-Based Lasers," *Astronautics and Aeronautics*, Vol. 10, No. 5, 1972, pp. 74–76.

[2]Birkan, M. A., "Laser Propulsion: Research Status and Needs," *Journal of Propulsion and Power*, Vol. 8, No. 2, 1992, pp. 354–360.

[3]Glumb, R. J., and Krier, H., "Concepts and Status of Laser-Supported Rocket Propulsion," *Journal of Spacecraft and Rockets*, Vol. 21, No. 1, 1984, pp. 70–79.

[4]Kare, J. T., "Pulsed Laser Propulsion for Low-Cost High-Volume Launch to Orbit," International Astronautics Federation Conference on Space Power, Cleveland, OH, June 1989.

[5]Kantrowitz, A., "Laser Propulsion to Earth Orbit; Has Its Time Come?" *Proceedings of the 1986 SDIO/DARPA Workshop on Laser Propulsion*, Vol. 2, 1986, pp. 49–56.

[6]Chern, J.-S., Hong, Z.-C., Cheng, W.-L., and Chang, C.-Y., "Trajectory Optimization for Two-Dimensional Ascent to GEO Using Laser Propulsion System," AAS/AIAA Astrodynamics Specialist Conference, Victoria, BC, Canada, Aug. 1993.

[7]Kare, J. T., "Trajectory Simulation for Laser Launching," *Proceedings of the 1986 SDIO/DARPA Workshop on Laser Propulsion*, Vol. 2, 1986, pp. 61–77.

[8]Pierson, B. L., "Sequential Quadratic Programming and Its Use in Optimal Control Model Comparisons," *Optimal Control Theory and Economic Analysis 3*, edited by G. Feichtinger, North-Holland, Amsterdam, 1988, pp. 175–193.

[9]Humble, W. E., "Optimal Trajectories for a Ground-to-Orbit Laser-Propelled Launch Vehicle," M.S. Thesis, Iowa State Univ., Ames, IA, 1993.

[10]Miele, A., *Flight Mechanics Volume 1: Theory of Flight Paths*, Addison–Wesley, Reading, MA, 1962, pp. 66–68.

[11]Truitt, R. W., *Hypersonic Aerodynamics*, Ronald, New York, 1959, pp. 13, 81–84.

[12]Pirri, A. N., Monsler, M. J., and Nebolsine, P. E., "Propulsion by Absorption of Laser Radiation," *AIAA Journal*, Vol. 12, No. 4, 1974, pp. 1254–1261.

[13]Kare, J. T., "Laser-Supported Detonation Waves and Pulsed Laser Propulsion," 17th International Shockwave and Shock Tube Symposium, Bethlehem, PA, July 1989.

[14]Pouliot, M. R., "CONOPT2: A Rapidly Convergent Constrained Trajectory Optimization Program for TRAJEX," General Dynamics, Convair Division, Rept. GDC-SP-82-008, San Diego, CA, 1982.